Marine Geology 413 (2019) 99–111

Contents lists available at ScienceDirect

Marine Geology

journal homepage: www.elsevier.com/locate/margo

Different origins of seafloor undulations in a submarine canyon system, northern South China Sea, based on their seismic character and relative location

Jian Li[a,b], Wei Li[a,b,*], Tiago M. Alves[c], Michele Rebesco[d], Wenhuan Zhan[a,b], Jie Sun[a], Neil C. Mitchell[e], Shiguo Wu[f]

[a] CAS Key Laboratory of Ocean and Marginal Sea Geology, South China Sea Institute of Oceanology, Chinese Academy of Sciences, Guangzhou 510301, PR China
[b] University of Chinese Academy of Sciences, Beijing 100049, PR China
[c] 3D Seismic Lab, School of Earth and Ocean Sciences, Cardiff University, Main Building, Park Place, Cardiff CF10 3AT, United Kingdom
[d] Instituto Nazionale di Oceanografia e di Geofisica Sperimentale (OGS), Borgo Grotta Gigante 42/C, Sgonico, 34010, Trieste, Italy
[e] School of Earth and Environmental Sciences, The University of Manchester, Manchester M13 9PL, UK
[f] Institute of Deep-sea Science and Engineering, Chinese Academy of Sciences, Sanya 572000, PR China

ARTICLE INFO

Editor: Shu Gao

Keywords:
South China Sea
Submarine canyons
Seafloor undulations
Bathymetry
Internal seismic character

ABSTRACT

High-resolution 2D and 3D seismic data are used to investigate the morphology, internal architecture and origin of widespread seafloor undulations in the eastern area of a submarine canyon system, northern South China Sea. The seafloor undulations reveal similar seafloor morphologies, and three different types (Types A, B and C) can be classified based on their relative locations and internal seismic characters. Types A and B are observed in the canyon areas, whereas Type C occurs in the canyon heads. Seismic reflections within Types A and C are continuous and have an upslope migrating trend, while Type B seafloor undulations are separated by listric faults. Our analysis reveals the origins of these three different types of seafloor undulations. Type A seafloor undulations are sediment waves formed by turbidity currents flowing through the submarine canyons. Gravity-driven submarine creep resulted in the formation of Type B seafloor undulations. Type C undulations are sediment waves generated by internal waves interacting with the continental slope. Our results provide information about the origin of widespread seafloor undulations in other submarine canyon systems. It is also of great significance to future risk assessments, as the study area now is one of the most active regions for hydrocarbon exploration in SE Asia.

1. Introduction

Seafloor undulations are one of the most widespread bedforms on both passive and active continental margins (Symons et al., 2016), revealing a wide range of morphologies, dimensions and sediment types (Ribó et al., 2018). Seafloor undulations are generated by a combination of depositional and erosional processes, and their crests comprise positive features relative to the surrounding seafloor (Symons et al., 2016). Seafloor undulations have been documented in a wide range of submarine settings, including on continental shelves (Belde et al., 2017), continental slopes (Ribó et al., 2018), continental rises (Gonthier et al., 2002), abyssal plains (Baldwin et al., 2017), the slopes of volcanic islands (Pope et al., 2018), and submarine canyons and channels (Gong et al., 2012). Seafloor undulations are commonly associated with sediment waves and sediment deformation under gravity-driven submarine creep (Wynn and Stow, 2002).

Sediment waves can be created by along-slope bottom currents, downslope turbidity currents or by a combination of both their processes (Wynn and Stow, 2002; Symons et al., 2016). Sediment waves formed by bottom currents are chiefly related to sediment drifts, with their wavelength and height reaching up to 10 km and 150 m, respectively (Flood et al., 1993; Wynn and Stow, 2002; Rebesco et al., 2007). Sediment waves formed by turbidity currents are common in channel levees, canyon and channel mouths, and typically reveal wavelengths and heights of up to 7 km and 80 m, respectively (Wynn and Stow, 2002). Sediment waves can also be generated by internal waves (Karl et al., 1986; Reeder et al., 2011; Ribó et al., 2016), and have been found in the heads of submarine canyons. Here, they show average wave

* Corresponding author at: CAS Key Laboratory of Ocean and Marginal Sea Geology, South China Sea Institute of Oceanology, Chinese Academy of Sciences, Guangzhou 510301, PR China.
E-mail address: wli@scsio.ac.cn (W. Li).

https://doi.org/10.1016/j.margeo.2019.04.007
Received 19 December 2018; Received in revised form 12 April 2019; Accepted 13 April 2019
Available online 19 April 2019

heights of 5 m and wavelengths of up to 650 m (Karl et al., 1986). Sediment waves have been widely documented on the northern South China Sea margin, especially in the Qiongdongnan (Jiang et al., 2013; Chen et al., 2017) and Taixinan Basin (Damuth, 1979; Gong et al., 2012; Kuang et al., 2014).

Apart from sediment waves formed by depositional and oceanographic processes, seafloor creep can also generate vast fields of undulations where slope gradients and sedimentation rates are relatively high (Lee and Chough, 2001; Faugères et al., 2002; Rebesco et al., 2009; Shillington et al., 2012; Li et al., 2016a). They can generate waves up to 10 km in length and 100 m in height (Wynn and Stow, 2002). Seafloor creeping can involve into large-scale submarine landslides, posing major geohazards to infrastructure such as telecommunication cables and pipelines (Lee and Chough, 2001; Shillington et al., 2012). Therefore, it is of great importance to correctly identify the origin of seafloor undulations, and to understand the tectonic, sedimentary and oceanographic setting in which they occur (Shillington et al., 2012; Belde et al., 2017).

A large-scale submarine canyon system, consisting of eighteen regular spaced, linear, sub-parallel submarine canyons, has been previously documented on the continental slope of the Pearl River Mouth Basin (He et al., 2014; Ma et al., 2015; Li et al., 2016b) (Figs. 1 and 2). The study area in this work is situated in the eastern part of this submarine canyon system at water depths between 600 and 1600 m (Fig. 2). Here, seafloor undulations are broadly distributed in the thalwegs, flanks and heads of the studied submarine canyons, and doubts still exist on their origin and formation processes. The seafloor undulations in the heads and flanks of the canyons have been proposed to reflect seafloor creep and landslides (He et al., 2014). However, Qiao et al. (2015) considered that seafloor undulations in the heads of the canyons relate to creep folds induced by soft sediment deformation, while waves in the lower segment of canyons are associated to turbidity currents overflowing their thalwegs. Additionally, seafloor undulations in the heads and on the flanks of canyons are caused by sediment deformation (Li et al., 2016b). Ma et al. (2015) also interpreted seafloor undulations in the heads and flanks of submarine canyons as failure scars. Notwithstanding these differing interpretations, it is of great importance to determine the exact origin and formation processes of these seafloor undulations, and their implications for future geohazard assessments. The study area is now one of the most active deep-water regions for hydrocarbon exploration on the northern South China Sea margin. In this study, a combination of 2D and 3D seismic data, and high-resolution bathymetry derived from 3D seismic data, are used to:

(a) investigate the morphology of the seafloor undulations;
(b) describe their detailed internal architectures on high-resolution seismic profiles;
(c) determine the origin of seafloor undulations in different segments of submarine canyons;
(d) discuss the implications of identifying seafloor undulations on continental margins.

2. Geological setting

The South China Sea (SCS) is located at the junction between the Pacific, the Indian-Australian, and the Eurasian tectonic plates, being the largest and deepest marginal sea in the western Pacific Ocean (Taylor and Hayes, 1980). Several major sedimentary basins occur along its northern margin, such as the Yinggehai, Qiongdongnan, Pearl River Mouth, and Taixinan Basins (Xie et al., 2006) (Fig. 1). As the largest deep-water basin in the northern South China Sea, the Pearl River Mouth Basin is also one of the most important petroliferous regions of China (Dong et al., 2009; Zhu et al., 2009).

The Baiyun Sag is an intraslope basin, with a water depth ranging from 200 to 2000 m, part of the larger Pearl River Mouth Basin (Zhu et al., 2010). A submarine canyon system consisting of eighteen submarine canyons is the most prominent geomorphologic feature of the Pearl River Mouth Basin (Figs. 1 and 2). This submarine canyon system records four evolutionary phases based on its internal seismic facies and spatial distribution (Ma et al., 2015): (1) small individual channels were initially formed in the middle of the Baiyun Sag (13.8–12.5 Ma); (2) channels were enlarged in a second stage because decreasing sediment

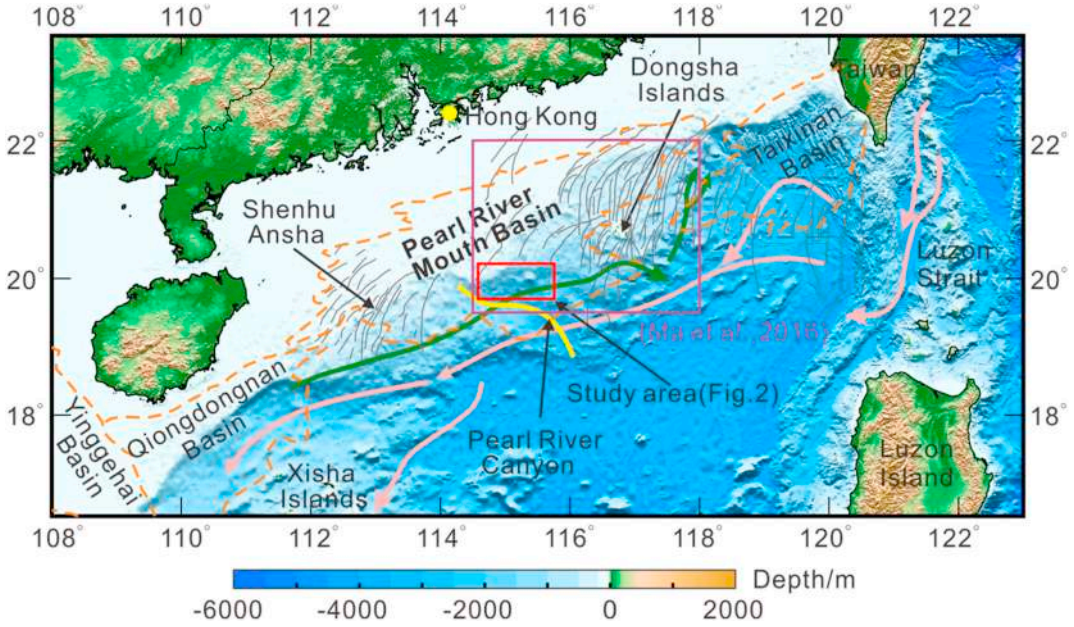

Fig. 1. Bathymetric map of the northern South China Sea margin. The orange dashed lines highlight the distribution of four major deep-water sedimentary basins. The yellow curve represents the location of the Pearl River Canyon. The grey curves represent internal waves observed in satellite imagery (extracted from Zhao et al., 2004; Li et al., 2011). The red box outlines the area enlarged in Fig. 2. The purple box represents extent of internal waves and the region of in situ current measurements (Ma et al., 2016). The green and pink arrows indicate the circulation pathways of intermediate and deep-water masses, respectively (modified after Chen et al., 2014). (For interpretation of the references to color in this figure legend, the reader is referred to the web version of this article.)

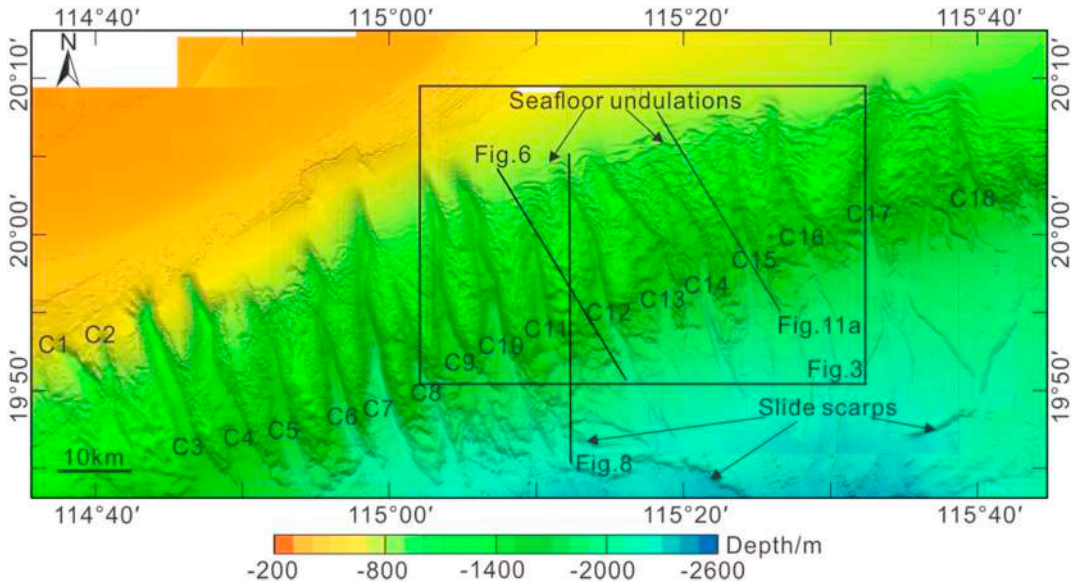

Fig. 2. High-resolution bathymetric map of the study area showing eighteen submarine canyons (C1 to C18) with a NW-SE orientation. Note that the heads of C9 to C18 show widespread seafloor undulations. Several slide scarps are clearly identified downslope from the submarine canyons. The black box represents the location of Fig. 3. The black lines show the location of the high-resolution seismic profiles in Figs. 6, 8 and 11.

input and stable tectonic subsidence in the Baiyun Sag increased the slope angle(12.5–10.5 Ma); (3) channels were broadly distributed and covered the entire Baiyun Sag due to a further decrease in sediment input, with the Dongsha Event later enhancing the flow of gravity currents (10.5–5.5 Ma); (4) channel incision ceased in the northeastern Baiyun Sag, while channels continued to develop in the study area to form modern features (5.5–0 Ma). In the study area, submarine canyons migrated unidirectionally to the NE from the middle Miocene to the present day due to the continued action of gravity and bottom currents (Zhu et al., 2010; Gong et al., 2013; Jiang et al., 2017; Gong et al., 2018).

Three major water masses exist at different depths on the northern South China Sea (Fig. 1).They comprise seasonal surface water masses (at < 350 m water depth), intermediate water masses (between 350 m and 1350 m water depth), and deep-water masses (at > 1350 m water depth) (Chen and Wang, 1998; Chen, 2005; Zhu et al., 2010; Gong et al., 2013). The study area is mainly affected by intermediate water and deep-water masses. Intermediate water, itself sourced from the North Pacific intermediate water, is considered to have an anti-cyclonic flow that was established in the late Miocene. It is characterised by salinity values between 34.35 and 34.43, with temperature ranging from 7 to 10 °C (Chen and Wang, 1998; Chen, 2005; Yang et al., 2010; Chen et al., 2014). Deep-water masses associated with the south-westward flow of the Northern Pacific Deep Water through the Luzon Strait, have a cyclonic circulation. Deep-water circulation was established in the late Miocene and gradually evolved into the modern pattern at ~1.0 Ma (Ludmann et al., 2005; Chen et al., 2014). At present, the velocity of deep-water masses generally varies between 0 and 2 cm/s based on in situ observations (Zhao et al., 2015).

Internal waves in the northern South China Sea are the largest waves documented in the world's oceans (Zhao et al., 2004; Li et al., 2011; Alford et al., 2015). Active internal wave fields in the northern South China Sea occur in the vicinity of the Dongsha Island and Shenhu Ansha shoal (Fig. 1). Remote sensing studies suggest that internal waves originate either from the local continental shelf break, or from the Luzon Strait on the eastern margin of the South China Sea, as a result of interactions between strong tides and local bathymetric features (Zhao et al., 2004; Li et al., 2008). These internal waves propagate into shallow waters and ultimately dissipate on the continental shelf (Li et al., 2011; Reeder et al., 2011; Ma et al., 2016).

3. Data and methods

The dataset used in this study consist of high-resolution bathymetric data derived from 3D seismic and 2D/3D seismic profiles (Figs. 2 and 3). The seismic data were acquired by China National Offshore Oil Corporation using a 3000-m long streamer with 240 channels. The 3D seismic volumes were collected with a sampling interval of 4 ms and processed with a bin spacing of 12.5 m × 25 m in their cross-line and inline directions, respectively. The frequency bandwidth of the seismic data is 30–45 Hz, providing an average vertical resolution of 8–10 m for the depth of occurrence of seafloor undulations. The vertical scale for all the seismic profiles used in this study is two-way travel time (TWT). Schlumberger's Geoframe® 4.5 software was used to visualise and interpret the seismic data.

The interpreted high-resolution bathymetric data covers the submarine canyon system of the Pearl River Mouth Basin in almost its entirety. Horizontal and vertical resolutions for the bathymetric data are ~100 m and 3–6 m, respectively. This resolution is sufficient to gather information on the dimensions, water depths and orientations of large-scale bedforms on the continental slope (Figs. 2 and 3).

4. Results

4.1. Seafloor morphology

4.1.1. General geomorphology

High-resolution bathymetric data shows that the continental slope has an inclination of ~2° between 300 m and 1600 m water depth (Figs. 2 and 3). The submarine canyons on the continental slope are connected to the wide continental shelf and deep-water basin, and are named in this work, from southwest to northeast, as C1 to C18 (Fig. 2). All submarine canyons are roughly perpendicular to the continental slope, and show a NW-SE orientation. Submarine canyons have lengths of 15–40 km, widths ranging from 2 to 5 km, and incision depths of 100–350 m (Fig. 2). Flanking strata between the submarine canyons become gradually narrower in the downslope direction (Fig. 2).

The high-resolution bathymetric map shows that the seafloor in the heads and flanks of the westernmost submarine canyons C1 to C8 is relatively smooth compared to the easternmost submarine canyons (C9–C18). The heads of canyons C9 to C18 are rough and characterised

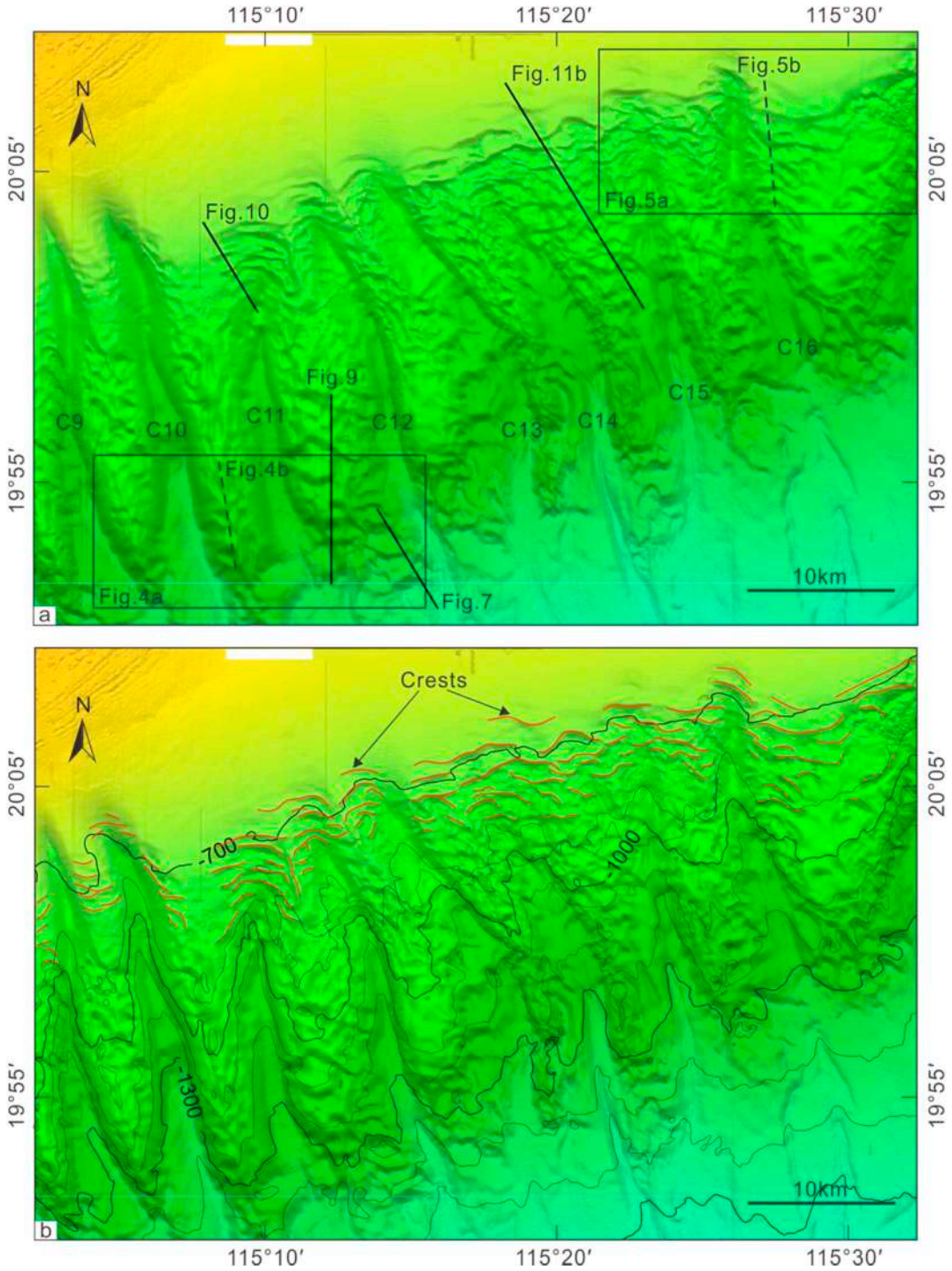

Fig. 3. (a) Bathymetric map illustrating the detailed morphology of the studied seafloor undulations. Seafloor undulations are mainly located at the heads and flanks of the submarine canyons. The black solid lines represent the locations of the 2D seismic profiles used in this study. The black dotted lines indicate the locations of bathymetric profiles show in Figs. 4b and 5b. (b) Distribution of the crests of seafloor undulations on the bathymetric map. The crests of the seafloor undulations are show in red and are parallel or sub-parallel to the bathymetric contours. The contour interval is 100 m. (For interpretation of the references to color in this figure legend, the reader is referred to the web version of this article.)

by widespread seafloor undulations. In addition, multiple slide scarps are observed in the downslope region of the submarine canyons (Fig. 2). The dimensions of these slide scarps range from hundreds of meters to several kilometres in length, and can be dozens of meters in height (Fig. 2).

4.1.2. Morphological description of the seafloor undulations

Seafloor undulations are chiefly located in the canyon thalwegs, flanks and heads of Canyons C9 to C18 (Figs. 2 and 3).

4.1.2.1. Seafloor undulations on the canyon flanks and lower slope. Compared to seafloor undulations at the canyon heads, undulations on the flanks and lower slope are smaller and more complex in plan view (Figs. 2 and 3). It is difficult to trace the crests of the seafloor undulations on the bathymetric map. However, the bathymetric profiles reveal that the wavelength (measured from trough

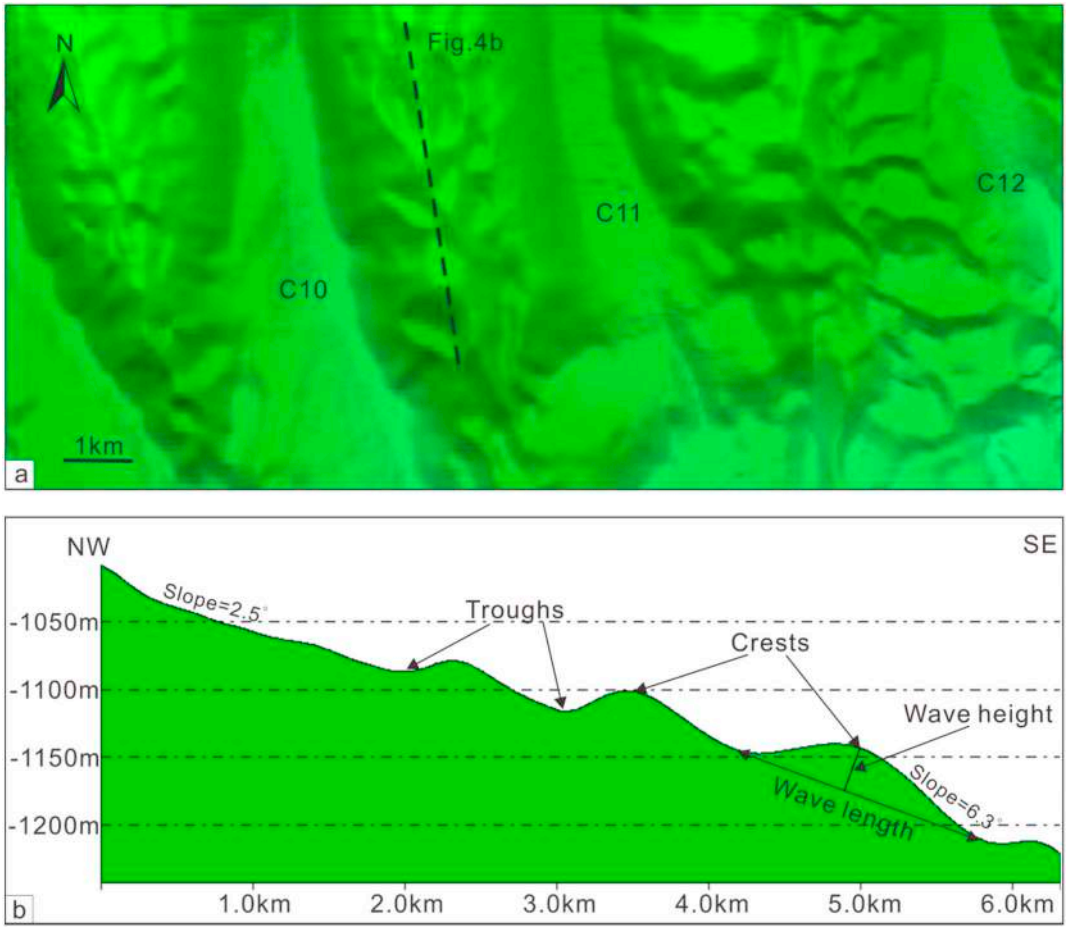

Fig. 4. (a) Bathymetric map revealing the detailed seafloor morphology of the lower flanks of submarine canyons, stressing the presence of widely distributed seafloor undulations. See Fig. 3 for the location of the bathymetric survey. (b) Bathymetric profile crossing the flank area between Canyon 10 and 11 and revealing multiple seafloor undulations. The wavelength and height of these seafloor undulations can reach up to 2 km and 100 m, respectively.

to trough) of seafloor undulations varies from 1 km to 2 km on the canyon flanks and lower slope (Fig. 4). Wave height ranges from 50 m to 100 m. In addition, a series of slide scars are observed on the canyon flanks (Fig. 2).

4.1.2.2. Seafloor undulations in the canyon heads. Multiple seafloor undulations were identified in the heads of the canyons at a water depth between 600 m and 900 m. Their strikes are roughly perpendicular to the canyon axis (Figs. 3 and 5a). The crests of the seafloor undulations (see red lines in Fig. 3b), are generally parallel or sub-parallel to the bathymetric contours. In addition, the crests of the seafloor undulations show no clear bifurcation in plan view. Topographic profiles crossing the head of the canyons reveal a variety of dimensions with wavelength ranging from 0.8 km to 1.5 km (Fig. 5). Wave height ranges from 20 m to50 m.

4.2. Seismic characteristics of the seafloor undulations

Several high-resolution seismic profiles crossing the thalwegs, flanks and heads of the submarine canyon system image the internal architecture of the seafloor undulations (Fig. 2). The seafloor undulations can therefore be divided into three main types, A, B and C, based on their internal architecture and relative locations in the submarine canyon system.

4.2.1. Type A seafloor undulations

Type A undulations are observed in the lower segments of the canyon thalwegs (Figs. 3, 6 and 7). The sedimentary succession affected by the undulations has a thickness of ~200 ms TWT (Fig. 7). Seismic profiles show that most seismic reflections are continuous, and can be traced from one wave to the next (Figs. 6 and 7). However, multiple mass-transport deposits (MTDs), characterised by discontinuous and chaotic internal seismic reflections, are also observed, proving that important sediment instability has occurred in the lower segment of the canyon thalwegs (Fig. 7).

Discrete undulations reveal an asymmetric morphology with gentle upslope flanks and steep downslope flanks (Fig. 7). They are commonly thicker on their upslope flanks. Undulations show a marked trend for upslope migration (Fig. 7b). Deeply buried undulations show relatively shorter upslope flanks and longer downslope flanks (Fig. 7). In contrast, the upslope flanks of shallow-buried undulations are longer than their downslope counterparts (Fig. 7). Downslope flanks also reveal erosional truncations in shallow-buried undulations (Fig. 7).

4.2.2. Type B seafloor undulations

Type B undulations occur on the canyon flanks, further upslope when compared to Type A. High-resolution seismic lines crossing the canyon flank between C11 and C12 reveal the internal architecture of Type B undulations (Figs. 2, 6, 8 and 9). The sedimentary succession affected by these undulations has a thickness of ~200 ms TWT. A series of high-amplitude (enhanced) seismic reflections can be identified along the base of the undulations (Figs. 6, 8 and 9a). They are usually distributed around, or above, focused fluid-flow structures such as gas chimneys (Figs. 8 and 9a).

Seismic reflections in Type B undulations are not continuous and cannot be traced across the troughs separating distinct sediment waves.

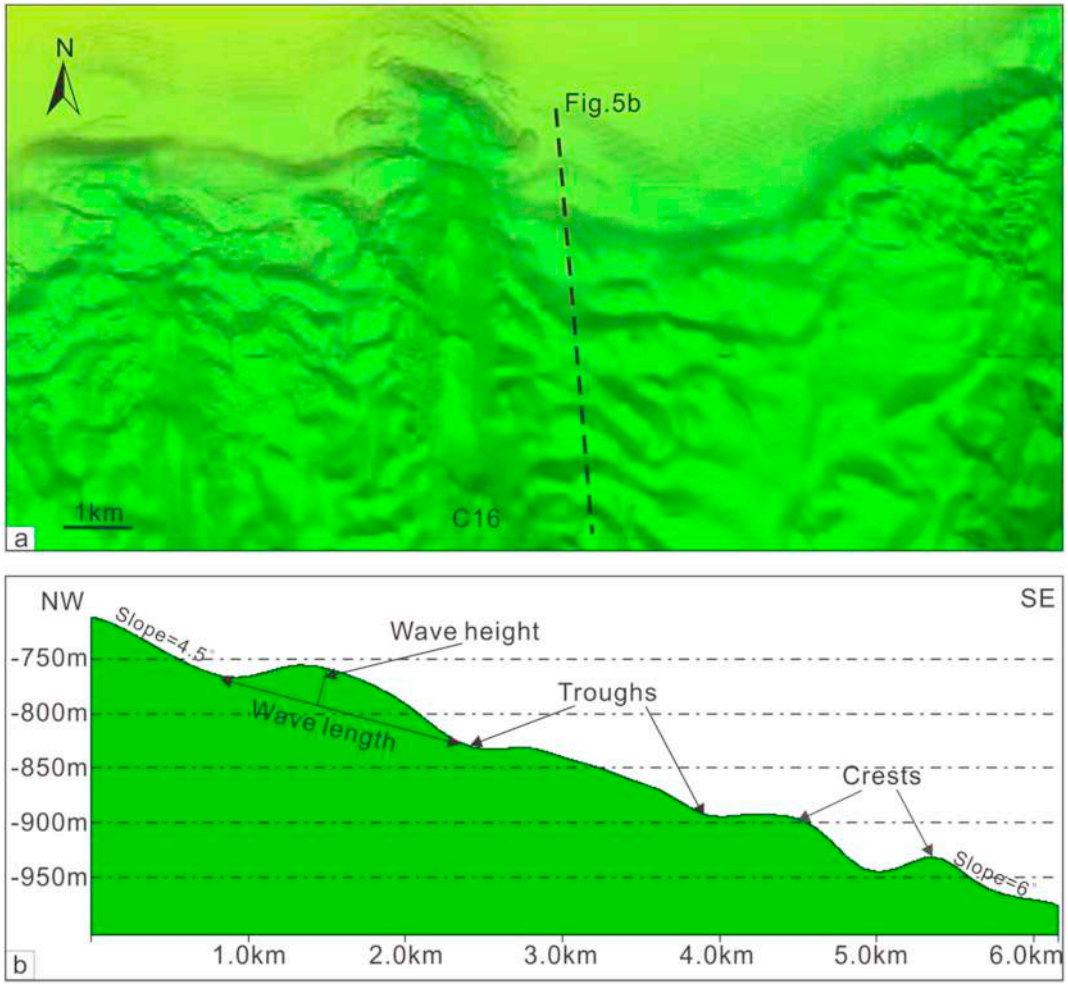

Fig. 5. (a) Bathymetric map highlighting the detailed seafloor morphology of the upper continental slope. Widespread seafloor undulations can be observed. See Fig. 3 for the location of the bathymetric survey. (b) Bathymetric profile crossing the upper ridge area between canyon 16 and 17, revealing the presence of multiple seafloor undulations. They can be up to 1.5 km in wavelength (trough to trough) and 50 m in height (maximum relief).

Most of these undulations are separated by listric faults (Figs. 6, 8 and 9). The troughs of the undulations are related to displacements of ~100 ms TWT along the fault planes (Fig. 9).

Type B undulations are characterised by their asymmetric morphology (Fig. 9). Upslope flanks reveal sub-parallel seismic reflections, whereas their downslope flanks are thin and show erosional truncation within shallow undulations (Fig. 9). The crests of Type B undulations also show an apparent upslope migration trend.

4.2.3. *Type C seafloor undulations*

Type C undulations are observed close to the heads of the canyons. The thickness of the strata affected by Type C undulations decreases from ~200 ms TWT to ~100 ms TWT in a downslope direction (Figs. 6, 10 and 11). Type C undulations are characterised by their wavy, asymmetric morphology and laterally continuous seismic reflections, although chaotic seismic reflections can also be identified due to the presence of MTDs (Fig. 11b). The upslope flanks of the undulations are

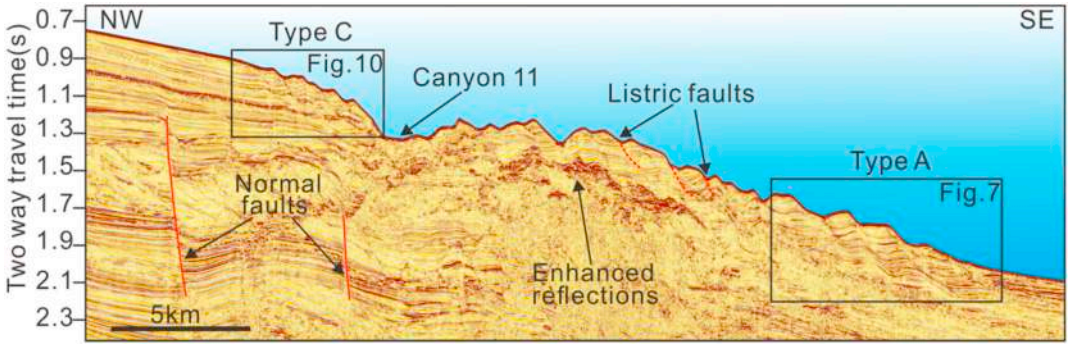

Fig. 6. Two-dimensional (2D) seismic line crossing the head of Canyon 11 and the flank area between C11 and C12 (Modified from Qiao et al. (2015); for location of the profile see Fig. 2). Several large-scale normal faults and listric faults can be distinguished, which are marked by red solid and dotted lines, respectively. Note the presence of high-amplitude enhanced seismic reflections beneath some of the seafloor undulations. (For interpretation of the references to color in this figure legend, the reader is referred to the web version of this article.)

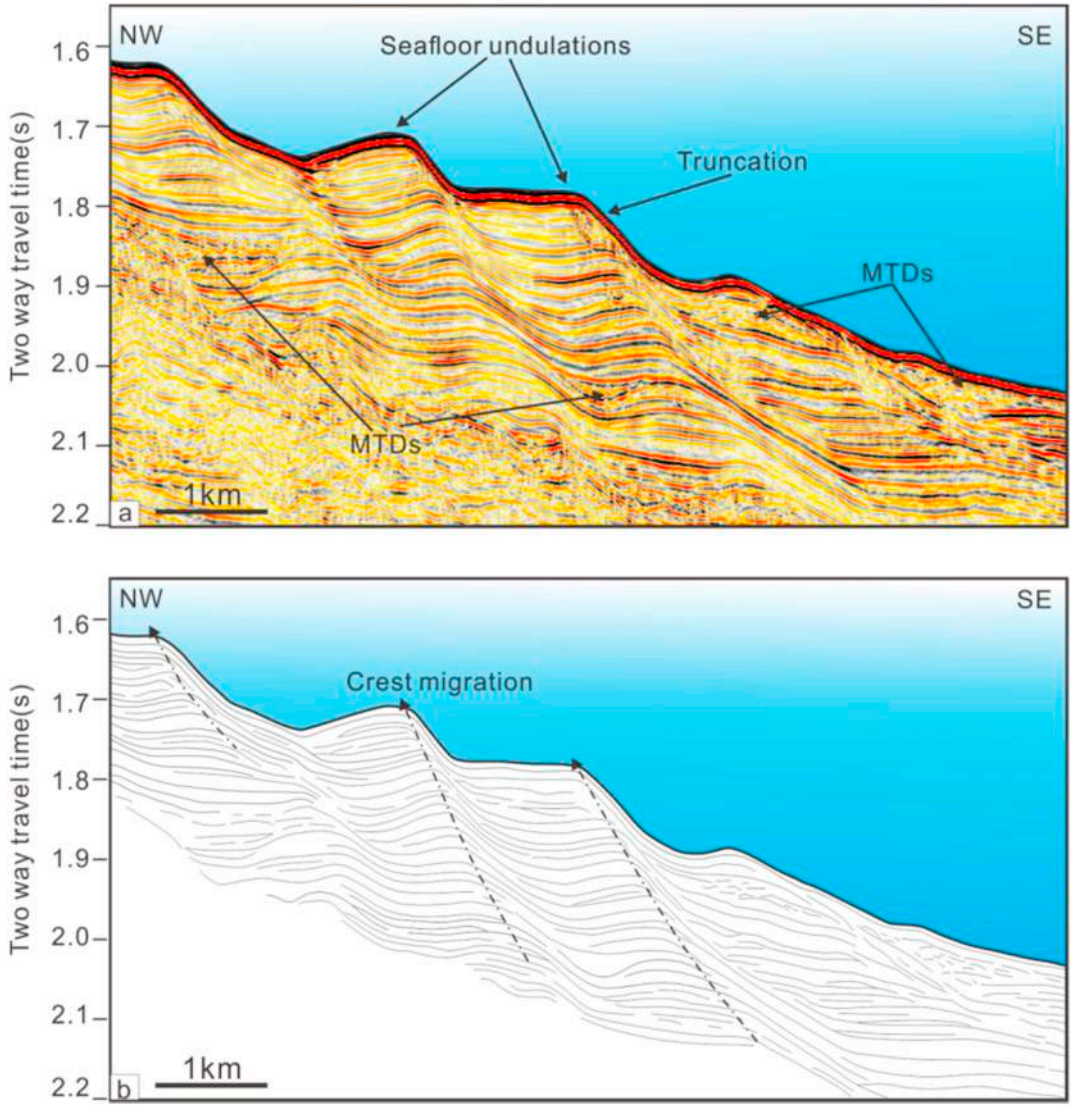

Fig. 7. (a) Zoomed section of the seismic profile in Fig. 6 revealing the detailed internal character of the seafloor undulations in the lower reach of the canyon flanks, between C11 and C12. Seafloor undulations are clearly observed on the seafloor and their crests show an upslope migration trend. Note that the downslope flanks of most of the undulated structures are steeper than their upslope counterparts. Several MTDs can be distinguished within the seafloor undulations. (b) Line-drawn interpretation of Fig. 7a revealing the internal seismic reflectors within the undulations, which are continuous across the troughs separating distinct undulations.

characterised by aggradation, whereas their downslope flanks are dominated by erosion and non-deposition. Thus, the crests of Type C undulations reveal an upslope migration trend with time. Note that some of shallow buried undulations reveal erosional truncation on their downslope flanks (Fig. 10a).

5. Discussion

5.1. Genesis of widespread seafloor undulations in a submarine canyon system

Seafloor undulations have been observed in submarine canyon systems all around the world (Gonthier et al., 2002; Gong et al., 2012; Ribó et al., 2018). Four main hypotheses have been proposed for their genesis based on the environment settings in which seafloor undulations occur, their morphological characteristics, and internal architectures. These four hypotheses include: (1) bottom currents (Masson et al., 2002; Baldwin et al., 2017; Belde et al., 2017); (2) turbidity currents (Lewis and Pantin, 2002; Normark et al., 2002; McCave, 2017); (3) internal waves (Karl et al., 1986; Droghei et al., 2016; Ma et al., 2016; Ribó et al., 2016); and (4) gravity-driven downslope submarine creeps (Lee and Chough, 2001; Shillington et al., 2012; Li et al., 2016a). In the following sections, the formation mechanisms of seafloor undulations are discussed for the study area based on the criteria proposed by Wynn and Stow (2002) and Symons et al. (2016).

5.1.1. Origin and formation process of Type A seafloor undulations(canyon thalwegs)

Turbidity currents are major downslope sediment transport processes, and are commonly identified in submarine canyons, channels and gullies (Shepard, 1981; Parker, 1982; Canals et al., 2006; Talling et al., 2015; Paull et al., 2018). Sediment waves generated by turbidity currents have been documented in regions such as the Monterey Fan channel (Normark et al., 1980), on the South Iberian Margin (Alves et al., 2003; Perez-Hernandez et al., 2014) and in the northern South China Sea (Gong et al., 2012; Jiang et al., 2013).

In the study area, Type A undulations are closely linked to the lower segments of the canyon thalwegs (Figs. 2, 6 and 7). Internal seismic reflections within the undulations are continuous and can be traced from one wave to the next (Figs. 6 and 7). Each undulation reveals an

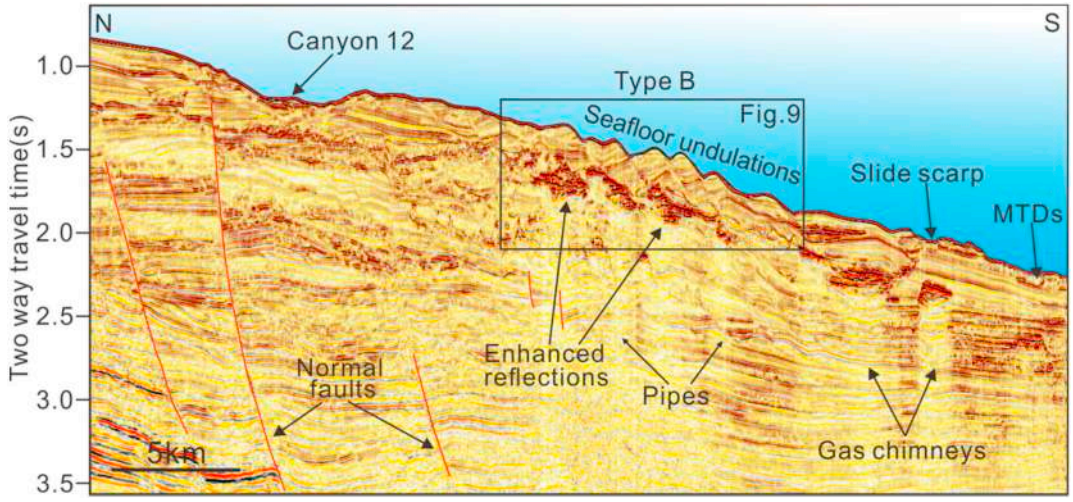

Fig. 8. High-resolution seismic profile crossing C12 and the canyon flank between C11 and C12 (for location of the profile see Fig. 2). A slide scarp and multiple seafloor undulations can be identified on the modern seafloor. Note the presence of gas chimneys, pipes and high-amplitude (enhanced) seismic reflections beneath the undulations.

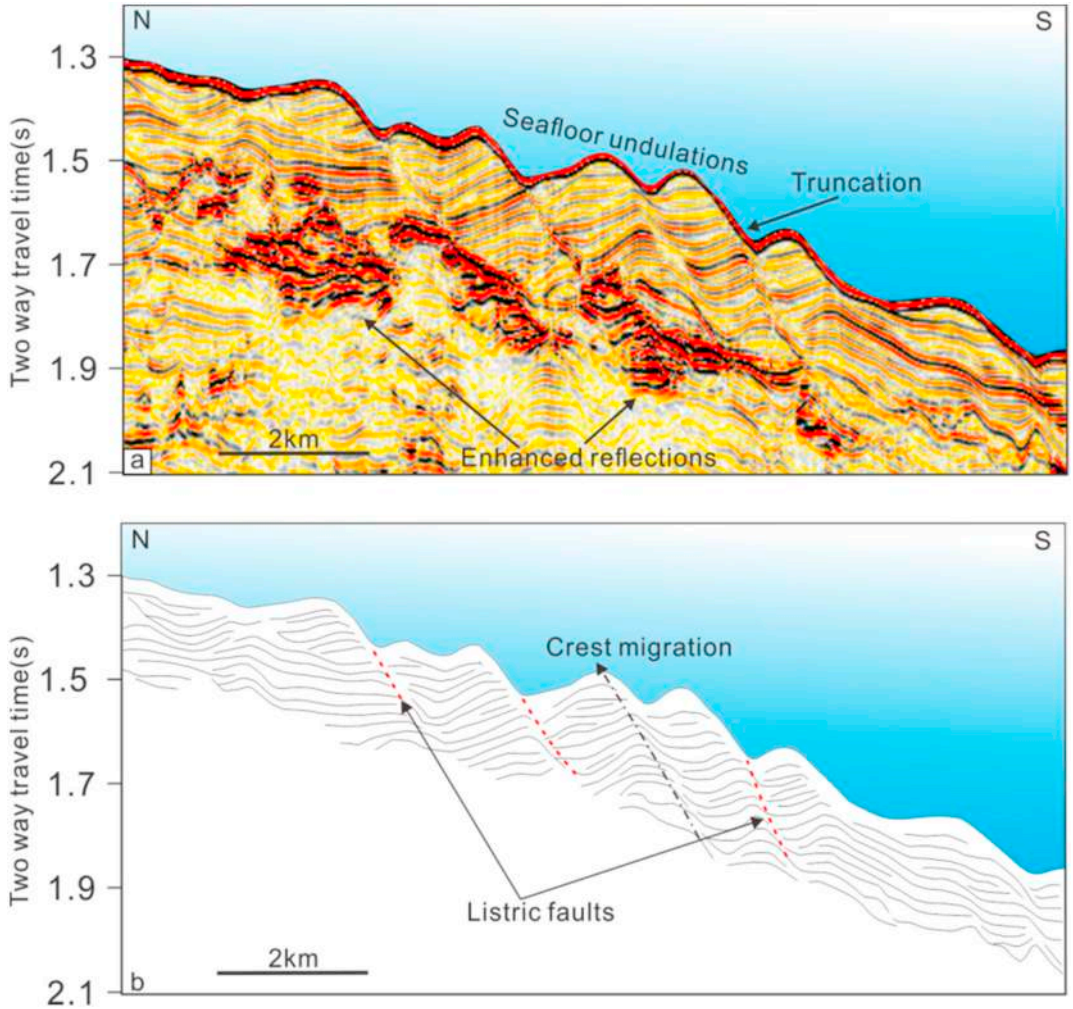

Fig. 9. (a) Zoomed section of the seismic profile in Fig. 8 showing the internal architecture of seafloor undulations on the canyon flank between C11 and C12. Seismic reflections within seafloor undulations are not continuous and cannot be traced across the troughs from one wave to the next. Most of the seafloor undulations are separated by small-scale listric faults. (b) Line-drawn interpretation of Fig. 9a illustrating the internal seismic reflections within the seafloor undulations, which are not continuous.

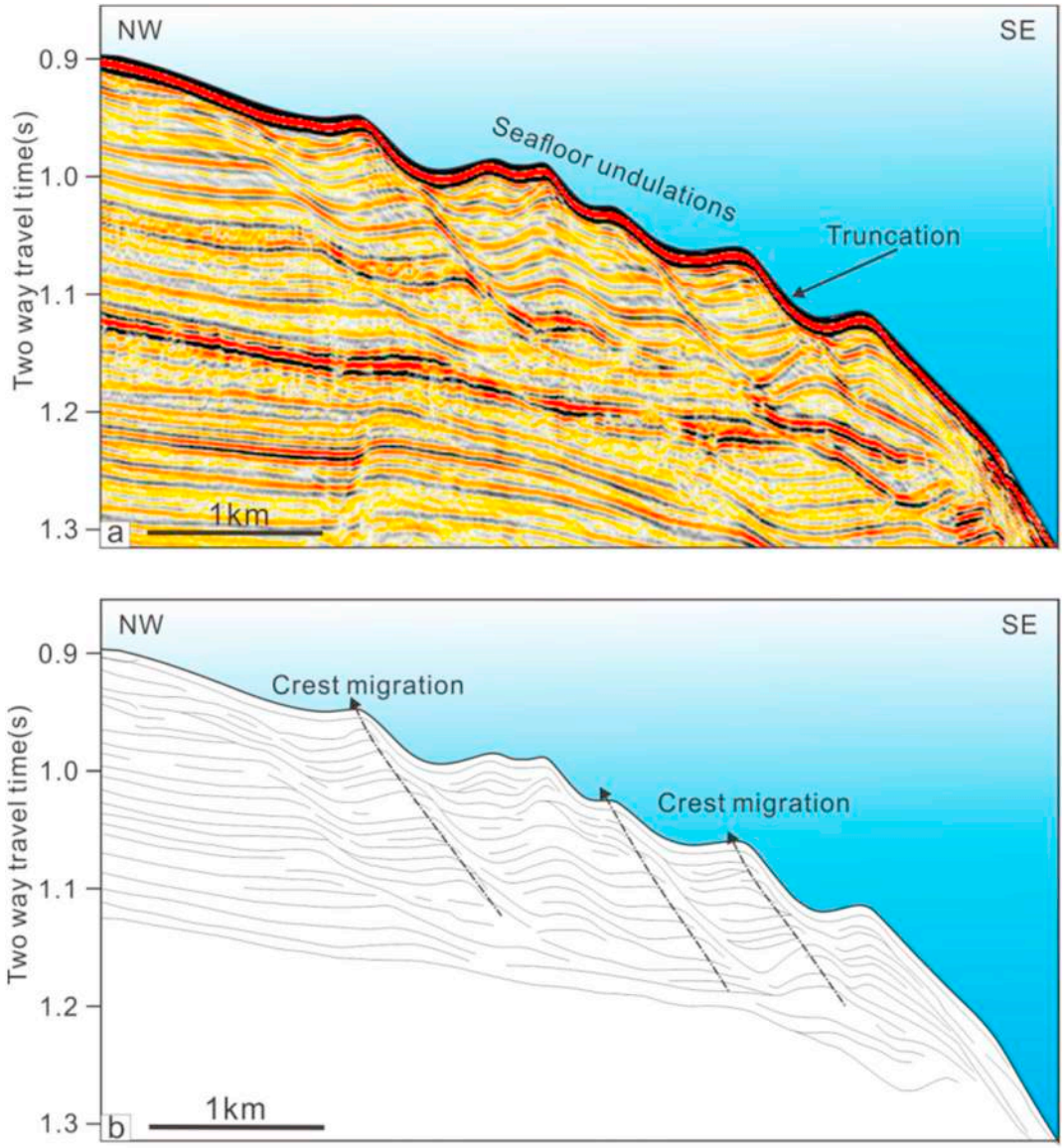

Fig. 10. (a) Zoomed section of the seismic profile in Fig. 6 showing the detailed internal architecture of sediment waves at the head of C11. Internal seismic reflections within the seafloor undulations are continuous and can be traced from one wave to the next. Note that the crests of the undulated structures reveal an upslope migration pattern. (b) Line-drawn interpretation of Fig. 10a highlighting that most of the internal reflectors crossing the different seafloor undulations are continuous.

asymmetric morphology, with gentle upslope flanks and steep downslope flanks (Fig. 7). All these undulations show a significant trend of upslope migration as their upslope flanks accumulate sediment more rapidly than their downslope flanks (Fig. 7). Based on criteria proposed by Wynn and Stow (2002), Type A undulations are similar to sediment waves generated by turbidity currents, e.g. the Selvagens sediment-wave field, NE Atlantic (Wynn et al., 2000), and the Hikurangi Trough east of New Zealand (Lewis and Pantin, 2002).

Our study area is located on the continental slope of the northern South China Sea. In this region, multiple submarine instability features, i.e. creeps, slumps and landslide complexes, are developed in an area incised by multiple submarine canyons (He et al., 2014; Chen et al., 2016). Previous studies suggest that turbidity currents are produced by the downslope transport of slumps and mass flows (Parker, 1982; Ercilla et al., 2002). Li et al. (2015) also suggest that slumps and mass flows occurred frequently in the past to generate turbidity currents in submarine canyon systems of the northern South China Sea margin. As discussed above, we infer that Type A undulations comprise sediment waves produced by turbidity currents associated with frequent slumping and mass wasting in the submarine canyons.

5.1.2. Origin and formation processes of Type B seafloor undulations (canyon flanks)

The internal seismic reflections within Type B undulations are not continuous, and cannot be traced across successive troughs separating the observed undulations (Figs. 6, 8 and 9). These troughs are commonly associated with listric faults (Figs. 6, 8 and 9). Undulations are generally thicker on their upslope flanks, and thinner (or even eroded) in their downslope flanks (Fig. 9). Seafloor undulations associated with listric faults have been documented by Faugères et al. (2002) and Gonthier et al. (2002). They were interpreted as reflecting gravity-driven downslope submarine creep. The basic conditions for the formation of submarine creeps have been summarised by Hill et al. (1982), including the presence of faulting and glide planes. When deforming

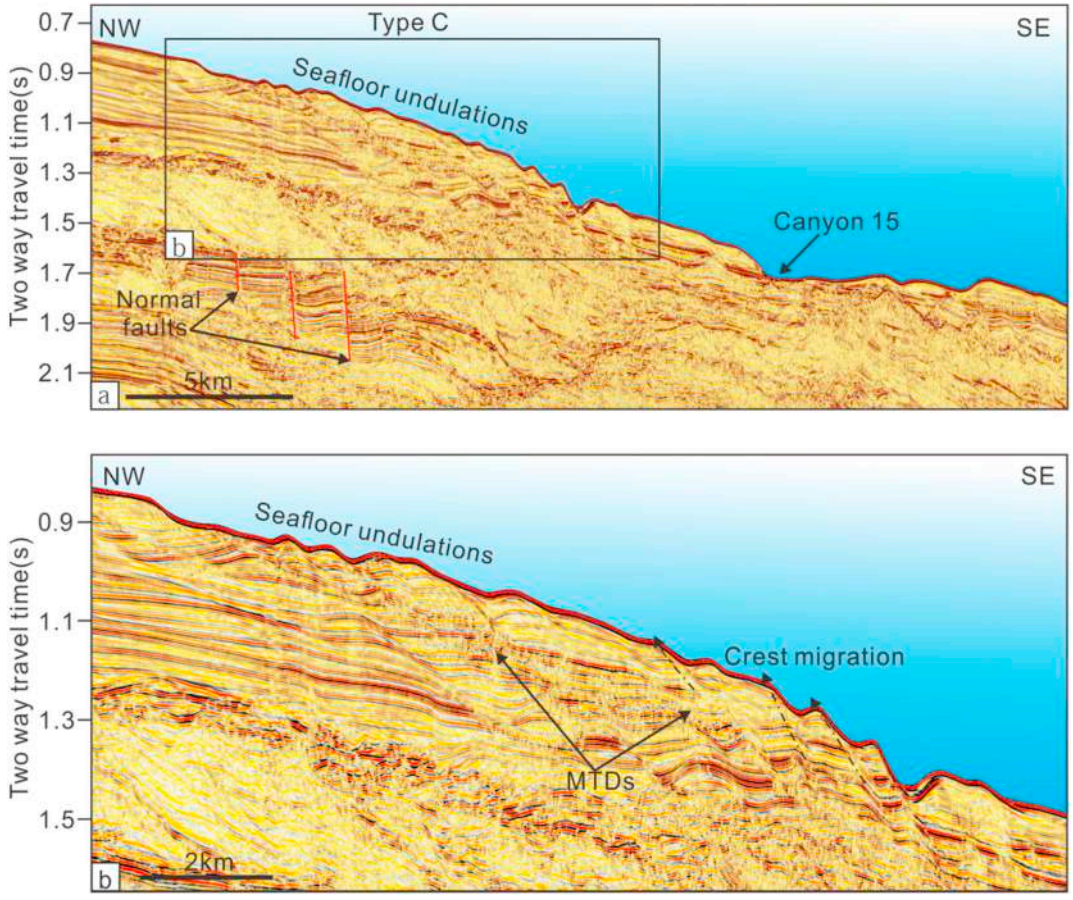

Fig. 11. (a) Two-dimensional (2D) seismic profile crossing C15 and the canyon flank between C14 and C15 (Modified from Qiao et al. (2015); see Fig. 2 for location of the profile). Multiple sediment waves are observed in the canyon head. (b) Zoomed section in Fig. 11b showing the internal architecture of sediment waves in the canyon head. Note that most of the sediment waves show an upslope migration trend. Several MTDs can be identified within the imaged sediment waves.

the sediments, a basal décollement zone is formed at the lower boundary of the strata. Listric faults act as glide planes for the displacement of the layered sediment. The regional slope gradient of submarine canyon systems varies from 1.5° to 2.5°, being ~1.6° on average (He et al., 2014; Li et al., 2016b).

In the study area, Type B undulations are mainly located on the canyon flanks, where slope gradients are steep (up to 8°). Sediment drilled on the flanks of the submarine canyons' lower segments consists of massive silty mud and a few sandy to silty intervals with weak layers (Qiao et al., 2015). Here, soft sediment deformation (submarine creep) is likely controlled by the slope gradient and strength of the sediment (Wynn and Stow, 2002). Due to progressing gravity-driven downslope deformation, the local accumulating of strain resulted in the development of local faults within sediment waves (Li et al., 2016a). Listric faults are developed within troughs, leading to significant displacement of adjacent undulations (Fig. 9). Thus, we interpret Type B undulations as the result of soft sediment deformation produced by gravity-driven downslope submarine creep.

Additionally, gas chimneys, pipes, large-scale normal faults and shallow gas are widespread on the lower slope of the interpreted submarine canyon system (Sun et al., 2012; Chen et al., 2016). Abundant acoustic anomalies, revealed as high-amplitude (enhanced) seismic reflections, can be observed close to the lower boundary of Type B undulations (Figs. 6, 8 and 9a). Elsewhere, similar enhanced seismic reflections have been associated with free gas and fluid accumulated in shallow strata (e.g. Sun et al., 2012, 2017). Gas chimneys, pipes and faults can act as pathways for the vertical migration of free gas and fluids (Sun et al., 2017). The presence of free gas and fluid increases overpressure in shallow strata, and reduces its shear strength until the creeping movements occur (e.g. Sultan et al., 2004; Urlaub et al., 2018).

5.1.3. Origin and formation process of the Type C seafloor undulations (canyon heads)

Type C undulations are identified in the canyon head areas (Figs. 3, 6, 10 and 11). The origin of these undulations has been interpreted in He et al. (2014), Qiao et al. (2015), Ma et al. (2015), and Li et al. (2016b). Some of these authors have suggested that seafloor undulations were generated by submarine soft-sediment deformation due to slow gravity-driven downslope creeping (He et al., 2014; Qiao et al., 2015). Others have stressed their association with failure scars and fissures (Ma et al., 2015; Li et al., 2016b). Obviously, debate still exists about the origin and formation processes of Type C undulations.

The internal seismic reflections of Type C undulations can be traced across the crests and troughs of each wave in the canyon heads (Figs. 6, 10 and 11). Such an internal seismic architecture suggests a depositional origin for Type C undulations, rather than creeping and faulting. These undulations are similar to sediment waves formed by turbidity currents on continental margins (Wynn and Stow, 2002). However, the study area is located on the upper continental slope and is connected to a wide continental shelf (Fig. 1). Type C undulations are widespread in the canyon heads, but there is no major sediment source nearby, capable of producing unconfined turbidity flows. For this reason, we consider unlikely Type C seafloor undulations to be generated by turbidity currents.

Previous studies have considered bottom currents as an important process forming sediment waves, such as in parts of the northeast Rockall Trough (Masson et al., 2002), the Caroline Basin in the West Pacific Ocean (Baldwin et al., 2017), and even in lakes (Ceramicola

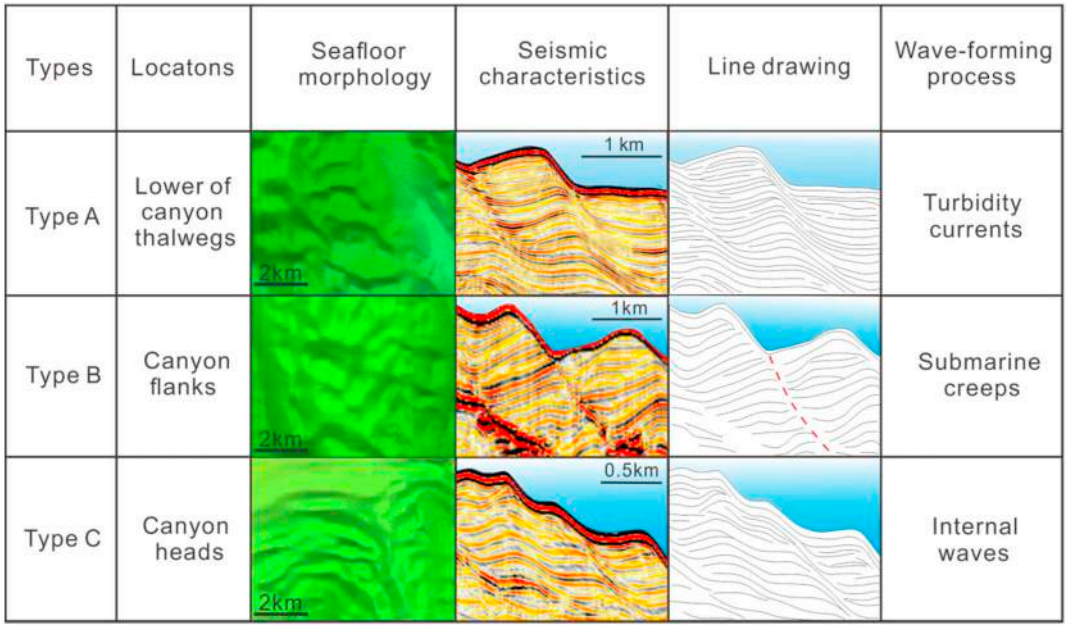

Fig. 12. Classification of three different types of seafloor undulations based on their location and origin. Representative seismic profiles and related line drawings illustrate the formation mechanisms of the seafloor undulations. Types A and B undulations are distributed in the canyon areas. The former are generated by turbidity currents, while the latter are generated by gravitational deformation processes (gravity-driven submarine creep). Type C undulations are mainly located at the heads of the submarine canyons and were generated by internal waves.

et al., 2001). Bottom currents, which are associated with the North Pacific intermediate water, affect the northern South China Sea at a water depth of 350–1350 m (Chen and Wang, 1998; Chen, 2005; Zhu et al., 2010; Chen et al., 2014). Bottom currents flow to the northeast along the continental slope and affect sedimentation in the studied submarine canyon system (Zhu et al., 2010; Gong et al., 2013; Jiang et al., 2017). Sediment waves formed by bottom currents are normally oblique to the continental slope, and their crests are aligned perpendicularly or obliquely to bottom current flows (Wynn and Stow, 2002). The crests of these sediment waves are also straight or slightly sinuous, such as this of sediment waves at the toe of the South China Sea continental slope, southwest Taiwan (Gong et al., 2012). In contrast with the latter geometries, the crests of Type C undulations are characterised by their curved shape in plan view, and are generally parallel or subparallel to the bathymetric contours (Figs. 2 and 3). We thus consider unlikely that bottom currents are responsible for the Type C undulations.

In recent years, an increasingly larger number of studies have considered internal waves as a formation mechanism for the generation of seafloor sediment waves (Karl et al., 1986; Reeder et al., 2011; Ribó et al., 2016). In fact, the South China Sea hosts the largest internal waves observed in the world's oceans (Li et al., 2011; Alford et al., 2015) (Fig. 1). They are the result of the interaction between strong tidal currents and the abrupt local bathymetry (Zhao et al., 2004; Li et al., 2008). Several fields of sediment wave have been reported on the continental shelf and slope off the Dongsha Islands, and they were interpreted as generated by internal waves interacting with the continental margin (Reeder et al., 2011; Ma et al., 2016). Our study area is just located on the western continental slope of the Dongsha Islands (Fig. 1), where internal waves have been documented by Ma et al. (2016). This indicates that the seafloor undulations in the canyon head areas might be produced by internal waves.

The breaking of internal waves on slope surfaces can create intense turbulence near the seafloor, generating local bottom currents with sufficient strength to resuspend and transport sediment (Bogucki and Redekopp, 1999; Ribbe and Holloway, 2001; Reeder et al., 2011). Moreover, internal waves' energy may be amplified at the canyon heads, as documented in the Hudson Canyon on the US Atlantic margin (Hotchkiss and Wunsch, 1982), and the Navarinsky Canyon in the Bering Sea (Karl et al., 1986). Consequently, when internal waves interact with the heads of the submarine canyons, they can become unstable, break and transfer wave energy to generate intense turbulence near the seafloor (Reeder et al., 2011; Pomar et al., 2012; Ribóet al., 2016). These seafloor-fluid mixtures, under the action of gravity, move downslope (Hotchkiss and Wunsch, 1982; Karl et al., 1986; Pomar et al., 2012).

A recent study by Ma et al. (2016) indicates that two types of sand waves can be discerned near the shelf break of the northern South China Sea. The crests of sand waves generated by internal tides are parallel to the isobaths, and are similar to the crests in the canyon heads of our study area (Fig. 3b). A primary question about the observed internal waves is how were they generated. Two sources of internal waves have been observed in the northern South China Sea. Based on remote sensing images, internal waves have been related to tidal action and Kuroshio current flow over the Luzon Strait on the eastern margin of the South China Sea (Zhao et al., 2004; Li et al., 2008). The other source of internal waves in the South China Sea is associated to the shelf break, which records incident trans-basin waves and internal tides (Guo et al., 2012; Reeder et al., 2011).

We infer that the Type C undulations identified in this work are most likely generated by internal waves. The source of these internal waves cannot be confirmed due to the lack of field measurements. In addition, when internal tides propagate, their energy dissipates because of inherent mixing processes in the ocean, accompanied by the generation of internal solitary waves (Guo et al., 2012). Therefore, more work is needed (e.g. in situ measurements and numerical simulations) to determine the source of the internal waves affecting the canyon head areas.

5.2. Significance of widespread seafloor undulations to geohazard assessments in the Pearl River Mouth Basin

The formation of seafloor undulations has been attributed to a variety of sedimentary, tectonic, and gravitational processes (Cartigny et al., 2011; Shillington et al., 2012). It is of great significance to correctly pinpoint the origin of seafloor undulations as they are essential

for understanding the oceanographic, sedimentary, and tectonic evolution of basins and margins and, particularly, for assessing geohazards related to slope instability (Shillington et al., 2012). The Pearl River Mouth Basin is one of the most important hydrocarbon-rich basins in the northern South China Sea and has been the focus of hydrocarbon expeditions and academic drilling (ODP Site 1148, IODP Expedition 349) for the past two decades (Li et al., 2005; Li et al., 2014). The submarine canyon area is also a target area for gas-hydrate exploration, e.g. the Shenhu area between Canyons C9 and C11 (Guan and Liang, 2018).

In this study, three different types of seafloor undulations (Types A, B and C) (Fig. 12) have been identified in the submarine canyons. These seafloor undulations show very similar morphologies on the bathymetric maps in Figs. 2 and 3. However, the internal architectures of these undulations are markedly different. Internal seismic reflections within Types A and C undulations are continuous and all show an apparent upslope migrating pattern (Figs. 7, 10 and 11). Types A and C sediment waves are purely generated by sedimentary processes (turbidity currents and internal waves). They are interpreted as the result of turbidity currents flowing within submarine canyons and internal waves interacting with the continental slope, respectively. However, their downslope flanks are quite steep (reaching 8°) and show lengths of up to 700 m. As such, the downslope flanks can be preferential areas for slope instability. Type B undulations are the seafloor manifestations of gravity-driven submarine creeping, and resemble the creep folds documented by Shillington et al. (2012) and Li et al. (2016a). They are commonly associated with listric faults, which act as potential glide planes for future slope instability (e.g. Li et al., 2016a). Resulting submarine landslides can pose catastrophic risks to oil and gas exploration and development (e.g. Piper et al., 1999). Therefore, more studies are required to determine the exact distribution of Type B seafloor undulations in the multiple submarine canyon systems of the northern South China Sea.

6. Conclusions

High-resolution 2D and 3D seismic data allowed us to investigate the morphology, internal architecture and origin of widespread seafloor undulations in the eastern area of a submarine canyon system, northern South China Sea. The main conclusions of this work are as follows:

(1) Seafloor undulations are distributed through canyon flanks, thalwegs and canyon-head areas. These seafloor undulations on the canyon flanks and thalwegs have wavelengths up to 2 km and heights up to 100 m. The wavelengths and wave heights on the canyon head areas are up to 1.5 km and 50 m, respectively.
(2) All identified undulations have similar morphologies on bathymetric maps, but the three different types of seafloor undulations (Types A, B and C) can be determined based on their relative locations and internal characters. Type A undulations occur mainly in the canyon thalwegs, and their internal seismic reflections are continuous, showing an apparent upslope migrating trend. Seismic reflections within Type B undulations are not continuous, but separated by listric faults. Type C undulations are observed in the canyon heads and their crests are roughly parallel to the local bathymetry.
(3) Types A and C undulations are sediment waves purely generated by sedimentary processes. Type A sediment waves are formed by turbidity currents flowing through the submarine canyons. Type C sediment waves most likely result from internal waves, which are amplified in the canyon heads, interacting with the continental slope. Type B undulations result from the gravity-driven (downslope) submarine creeping.
(4) To correctly identify the origin, formation processes and distribution of sediment waves in the submarine canyon systems off South China will be of great significance for future geohazard assessments in what is a hydrocarbon-rich basin of the South China Sea.

Acknowledgements

We thank China National Offshore Oil Corporation for their permission to release the seismic data. This work was financially supported by the National Scientific Foundation of China (Grant No. 41876054) and the Key Laboratory of Ocean and Marginal Sea Geology, Chinese Academy of Sciences (Grant No. OMG18-09). We thank Prof. Puig Pere and Prof. Mike Blum for valuable discussion. Dr. Wei Li is funded by the CAS Pioneer Hundred Talents Program. This paper benefited from the constructive comments of the editor (Prof. Shu Gao), Dr. Chenglin Gong and two anonymous reviewers.

References

Alford, M.H., Peacock, T., MacKinnon, J.A., Nash, J.D., Buijsman, M.C., Centuroni, L.R., Chao, S.-Y., Chang, M.-H., Farmer, D.M., Fringer, O.B., Fu, K.-H., Gallacher, P.C., Graber, H.C., Helfrich, K.R., Jachec, S.M., Jackson, C.R., Klymak, J.M., Ko, D.S., Jan, S., Johnston, T.M.S., Legg, S., Lee, I.H., Lien, R.-C., Mercier, M.J., Moum, J.N., Musgrave, R., Park, J.-H., Pickering, A.I., Pinkel, R., Rainville, L., Ramp, S.R., Rudnick, D.L., Sarkar, S., Scotti, A., Simmons, H.L., St Laurent, L.C., Venayagamoorthy, S.K., Wang, Y.-H., Wang, J., Yang, Y.J., Paluszkiewicz, T., Tang, T.-Y., 2015. The formation and fate of internal waves in the South China Sea. Nature 521, 65–U381.

Alves, T.M., Gawthorpe, R.L., Hunt, D.W., Monteiro, J.H., 2003. Cenozoic tectono-sedimentary evolution of the western Iberian margin. Mar. Geol. 195, 75–108.

Baldwin, K.E., Mountain, G.S., Rosenthal, Y., 2017. Sediment waves in the Caroline Basin suggest evidence for Miocene shifts in bottom water flow in the western equatorial Pacific. Mar. Geol. 393, 194–202.

Belde, J., Reuning, L., Back, S., 2017. Bottom currents and sediment waves on a shallow carbonate shelf, Northern Carnarvon Basin, Australia. Cont. Shelf Res. 138, 142–153.

Bogucki, D.J., Redekopp, L.G., 1999. A mechanism for sediment resuspension by internal solitary waves. Geophys. Res. Lett. 26, 1317–1320.

Canals, M., Puig, P., de Madron, X.D., Heussner, S., Palanques, A., Fabres, J., 2006. Flushing submarine canyons. Nature 444, 354–357.

Cartigny, M.J.B., Postma, G., van den Berg, J.H., Mastbergen, D.R., 2011. A comparative study of sediment waves and cyclic steps based on geometries, internal structures and numerical modeling. Mar. Geol. 280, 40–56.

Ceramicola, S., Rebesco, M., De Batist, M., Khlystov, O., 2001. Seismic evidence of small-scale lacustrine drifts in Lake Baikal (Russia). Mar. Geophys. Res. 22, 445–464.

Chen, C.T.A., 2005. Tracing tropical and intermediate waters from the South China Sea to the Okinawa Trough and beyond. J. Geophys. Res. Oceans 110, C05012.

Chen, C.T.A., Wang, S.L., 1998. Influence of intermediate water in the western Okinawa Tough by the outflow from the South China Sea. J. Geophys. Res. Oceans 103, 12683–12688.

Chen, H., Xie, X.N., Van Rooij, D., Vandorpe, T., Su, M., Wang, D.X., 2014. Depositional characteristics and processes of alongslope currents related to a seamount on the northwestern margin of the Northwest Sub-Basin, South China Sea. Mar. Geol. 355, 36–53.

Chen, D.X., Wang, X.J., Völker, D., Wu, S.G., Wang, L., Li, W., Li, Q.P., Zhu, Z.Y., Li, C.L., Qin, Z.L., Sun, Q.L., 2016. Three dimensional seismic studies of deep-water hazard-related features on the northern slope of South China Sea. Mar. Pet. Geol. 77, 1125–1139.

Chen, H.J., Zhan, W.H., Li, L.Q., Wen, M.M., 2017. Occurrence of submarine canyons, sediment waves and mass movements along the northern continental slope of the South China Sea. J. Earth Syst. Sci. 126, 73.

Damuth, J.E., 1979. Migrating sediment waves created by turbidity currents in the northern South China Basin. Geology 7, 520–523.

Dong, D.D., Zhang, G.C., Zhong, K., Yuan, S.Q., Wu, S.G., 2009. Tectonic Evolution and Dynamics of Deepwater Area of Pearl River Mouth Basin, Northern South China Sea. J. Earth Sci. 20, 147–159.

Droghei, R., Falcini, F., Casalbore, D., Martorelli, E., Mosetti, R., Sannino, G., Santoleri, R., Chiocci, F.L., 2016. The role of Internal Solitary Waves on deep-water sedimentary processes: the case of up-slope migrating sediment waves off the Messina Strait. Sci. Rep. 6. https://doi.org/10.1038/srep36376.

Ercilla, G., Wynn, R.B., Alonso, B., Baraza, J., 2002. Initiation and evolution of turbidity current sediment waves in the Magdalena turbidite system. Mar. Geol. 192, 153–169.

Faugères, J.C., Gonthier, E., Mulder, T., Kenyon, N., Cirac, P., Griboulard, R., Berne, S., Lesuave, R., 2002. Multi-process generated sediment waves on the Landes Plateau (Bay of Biscay, North Atlantic). Mar. Geol. 182, 279–302.

Flood, R.D., Shor, A.N., Manley, P.L., 1993. Morphology of abyssal mudwaves at Project MUDWAVES sites in the Argentine Basin. Deep-Sea Res. II Top. Stud. Oceanogr. 40, 859–888.

Gong, C.L., Wang, Y.M., Peng, X.C., Li, W.G., Qiu, Y., Xu, S., 2012. Sediment waves on the South China Sea Slope off southwestern Taiwan: Implications for the intrusion of the Northern Pacific Deep Water into the South China Sea. Mar. Pet. Geol. 32, 95–109.

Gong, C.L., Wang, Y.M., Zhu, W.L., Li, W.G., Xu, Q., 2013. Upper Miocene to Quaternary unidirectionally migrating deep-water channels in the Pearl River Mouth Basin, northern South China Sea. AAPG Bull. 97, 285–308.

Gong, C.L., Wang, Y.M., Rebesco, M., Salon, S., Steel, R.J., 2018. How do turbidity flows interact with contour currents in unidirectionally migrating deep-water channels? Geology 46, 551–554.

Gonthier, E., Faugères, J.C., Gervais, A., Ercilla, G., Alonso, B., Baraza, J., 2002. Quaternary sedimentation and origin of the Orinoco sediment–wave field on the Demerara continental rise (NE margin of South America). Mar. Geol. 192, 189–214.
Guan, J.A., Liang, D.Q., 2018. Discussion on the rapid formation mechanism and evolution process of methane hydrate-bearing sediments in Shenhu Area of northern South China Sea. Mar. Pet. Geol. 91, 225–235.
Guo, P., Fang, W.D., Liu, C.J., Qiu, F.W., 2012. Seasonal characteristics of internal tides on the continental shelf in the northern South China Sea. J. Geophys. Res. Oceans 117 (C04023).
He, Y., Zhong, G.F., Wang, L.L., Kuang, Z.G., 2014. Characteristics and occurrence of submarine canyon-associated landslides in the middle of the northern continental slope, South China Sea. Mar. Pet. Geol. 57, 546–560.
Hill, P.R., Moran, K.M., Blasco, S.M., 1982. Creep deformation of slope sediments in the Canadian Beaufort Sea. Geo-Mar. Lett. 2, 163–170.
Hotchkiss, F.S., Wunsch, C., 1982. Internal waves in Hudson Canyon with possible geological implications. Deep Sea Res. Part A 29, 415–442.
Jiang, T., Xie, X.N., Wang, Z.F., Li, X.S., Zhang, Y.Z., Sun, H., 2013. Seismic features and origin of sediment waves in the Qiongdongnan Basin, northern South China Sea. Mar. Geophys. Res. 34, 281–294.
Jiang, J., Shi, H.S., Lin, C.S., Zhang, Z.T., Wei, A., Zhang, B., Shu, L.F., Tian, H.X., Tao, Z., Liu, H.Y., 2017. Sequence architecture and depositional evolution of the Late Miocene to quaternary northeastern shelf margin of the South China Sea. Mar. Pet. Geol. 81, 79–97.
Karl, H.A., Cacchione, D.A., Carlson, P.R., 1986. Internal-wave currents as a mechanism to account for large sand waves in Navarinsky Canyon head, Bering Sea. J. Sediment. Petrol. 56, 706–714.
Kuang, Z.G., Zhong, G.F., Wang, L.L., Guo, Y.Q., 2014. Channel-related sediment waves on the eastern slope offshore Dongsha Islands, northern South China Sea. J. Asian Earth Sci. 79, 540–551.
Lee, S.H., Chough, S.K., 2001. High-resolution (2–7 kHz) acoustic and geometric characters of submarine creep deposits in the South Korea Plateau, East Sea. Sedimentology 48, 629–644.
Lewis, K.B., Pantin, H.M., 2002. Channel-axis, overbank and drift sediment waves in the southern Hikurangi Trough, New Zealand. Mar. Geol. 192, 123–151.
Li, Q.Y., Jian, Z.M., Su, X., 2005. Late Oligocene rapid transformations in the South China Sea. Mar. Micropaleontol. 54, 5–25.
Li, X.F., Zhao, Z.X., Pichel, W.G., 2008. Internal solitary waves in the northwestern South China Sea inferred from satellite images. Geophys. Res. Lett. 35. https://doi.org/10.1029/2008GL034272.
Li, D., Chen, X., Liu, A., 2011. On the generation and evolution of internal solitary waves in the northwestern South China Sea. Ocean Model 40, 105–119.
Li, C.F., Xu, X., Lin, J., Sun, Z., Zhu, J., Yao, Y.J., Zhao, X.X., Liu, Q.S., Kulhanek, D.K., Wang, J., Song, T.R., Zhao, J.F., Qiu, N., Guan, Y.X., Zhou, Z.Y., Williams, T., Bao, R., Briais, A., Brown, E.A., Chen, Y.F., Clift, P.D., Colwell, F.S., Dadd, K.A., Ding, W.W., Almeida, I.H., Huang, X.L., Hyun, S., Jiang, T., Koppers, A.A.P., Li, Q.Y., Liu, C.L., Liu, Z.F., Nagai, R.H., Peleo-Alampay, A., Su, X., Tejada, M.L.G., Trinh, H.S., Yeh, Y.C., Zhang, C.L., Zhang, F., Zhang, G.L., 2014. Ages and magnetic structures of the South China Sea constrained by deep tow magnetic surveys and IODP Expedition 349. Geochem. Geophys. Geosyst. 15, 4958–4983.
Li, X.S., Liu, L.J., Li, J.G., Gao, S., Zhou, Q.J., Su, T.Y., 2015. Mass movements in small canyons in the northeast of Baiyun Deepwater area, north of the South China Sea. Acta Oceanol. Sin. 34, 35–42.
Li, W., Alves, T.M., Wu, S.G., Rebesco, M., Zhao, F., Mi, L.J., Ma, B.J., 2016a. A giant, submarine creep zone as a precursor of large-scale slope instability offshore the Dongsha Islands (South China Sea). Earth Planet. Sci. Lett. 451, 272–284.
Li, X.S., Zhou, Q.J., Su, T.Y., Liu, L.J., Gao, S., Zhou, S.W., 2016b. Slope-confined submarine canyons in the Baiyun deep-water area, northern South China Sea: variation in their modern morphology. Mar. Geophys. Res. 37, 95–112.
Ludmann, T., Wong, H.K., Berglar, K., 2005. Upward flow of North Pacific Deep Water in the northern South China Sea as deduced from the occurrence of drift sediments. Geophys. Res. Lett. 32, L05614.
Ma, B.J., Wu, S.G., Sun, Q.L., Mi, L.J., Wang, Z.Z., Tian, J., 2015. The late Cenozoic deep-water channel system in the Baiyun Sag, Pearl River Mouth Basin: Development and tectonic effects. Deep-Sea Res. II Top. Stud. Oceanogr. 122, 226–239.
Ma, X.C., Yan, J., Hou, Y.J., Lin, F.L., Zheng, X.F., 2016. Footprints of obliquely incident internal solitary waves and internal tides near the shelf break in the northern South China Sea. J. Geophys. Res. Oceans 121, 8706–8719.
Masson, D.G., Howe, J.A., Stoker, M.S., 2002. Bottom-current sediment waves, sediment drifts and contourites in the northern Rockall Trough. Mar. Geol. 192, 215–237.
McCave, I.N., 2017. Formation of sediment waves by turbidity currents and geostrophic flows: a discussion. Mar. Geol. 390, 89–93.
Normark, W.R., Hess, G.R., Stow, D.A.V., Bowen, A.J., 1980. Sediment waves on the Monterey fan levee: a preliminary physical interpretation. Mar. Geol. 37, 1–18.
Normark, W.R., Piper, D.J.W., Posamentier, H., Pirmez, C., Migeon, S., 2002. Variability in form and growth of sediment waves on turbidite channel levees. Mar. Geol. 192, 23–58.
Parker, G., 1982. Conditions for the ignition of catastrophically erosive turbidity currents. Mar. Geol. 46, 307–327.
Paull, C.K., Talling, P.J., Maier, K.L., Parsons, D., Xu, J.P., Caress, D.W., Gwiazda, R., Lundsten, E.M., Anderson, K., Barry, J.P., Chaffey, M., O'Reilly, T., Rosenberger, K.J., Gales, J.A., Kieft, B., McGann, M., Simmons, S.M., McCann, M., Sumner, E.J., Clare, M.A., Cartigny, M.J., 2018. Powerful turbidity currents driven by dense basal layers. Nat. Commun. 9, 4114.
Perez-Hernandez, S., Comas, M.C., Escutia, C., 2014. Morphology of turbidite systems within an active continental margin (the Palomares Margin, western Mediterranean). Geomorphology 219, 10–26.
Piper, D.J.W., Cochonat, P., Morrison, M., 1999. The sequence of events around the epicentre of the 1929 grand banks earthquake: initiation of debris flows and turbidity currents inferred from sidescan sonar. Sedimentology 46, 79–97.
Pomar, L., Morsilli, M., Hallock, P., Bádenas, B., 2012. Internal waves, an under-explored source of turbulence events in the sedimentary record. Earth Sci. Rev. 111, 56–81.
Pope, E.L., Jutzeler, M., Cartigny, M.J.B., Shreeve, J., Tailing, P.J., Wright, I.C., Wysoczanski, R.J., 2018. Origin of spectacular fields of submarine sediment waves around volcanic islands. Earth Planet. Sci. Lett. 493, 12–24.
Qiao, S.H., Su, M., Kuang, Z.G., Yang, R., Liang, J.Q., Wu, N.Y., 2015. Canyon-related undulation structures in the Shenhu area, northern South China Sea. Mar. Geophys. Res. 36, 243–252.
Rebesco, M., Camerlenghi, A., Volpi, V., Neagu, C., Accettella, D., Lindberg, B., Cova, A., Zgur, F., 2007. Interaction of processes and importance of contourites: insights from the detailed morphology of sediment Drift 7, Antarctica. Geol. Soc. Lond., Spec. Publ. 276, 95–110.
Rebesco, M., Neagu, R.C., Cuppari, A., Muto, F., Accettella, D., Dominici, R., Cova, A., Romano, C., Caburlotto, A., 2009. Morphobathymetric analysis and evidence of submarine mass movements in the western Gulf of Taranto (Calabria margin, Ionian Sea). Int. J. Earth Sci. 98, 791–805.
Reeder, D.B., Ma, B.B., Yang, Y.J., 2011. Very large subaqueous sand dunes on the upper continental slope in the South China Sea generated by episodic, shoaling deep-water internal solitary waves. Mar. Geol. 279, 12–18.
Ribbe, J., Holloway, P.E., 2001. A model of suspended sediment transport by internal tides. Cont. Shelf Res. 21, 395–422.
Ribó, M., Puig, P., Muñoz, A., Lo Iacono, C., Masqué, P., Palanques, A., Acosta, J., Guillén, J., Gómez Ballesteros, M., 2016. Morphobathymetric analysis of the large fine-grained sediment waves over the Gulf of Valencia continental slope (NW Mediterranean). Geomorphology 253, 22–37.
Ribó, M., Durán, R., Puig, P., Van Rooij, D., Guillén, J., Masqué, P., 2018. Large sediment waves over the Gulf of Roses upper continental slope (NW Mediterranean). Mar. Geol. 399, 84–96.
Shepard, F.P., 1981. Submarine Canyons: Multiple Causes and Long-Time Persistence. AAPG Bull. Am. Assoc. Pet. Geol. 65, 1062–1077.
Shillington, D.J., Seeber, L., Sorlien, C.C., Steckler, M.S., Kurt, H., Dondurur, D., Cifci, G., Imren, C., Cormier, M.H., McHugh, C.M.G., Gurcay, S., Poyraz, D., Okay, S., Atgin, O., Diebold, J.B., 2012. Evidence for widespread creep on the flanks of the Sea of Marmara transform basin from marine geophysical data. Geology 40, 439–442.
Sultan, N., Cochonat, P., Canals, M., Cattaneo, A., Dennielou, B., Haflidason, H., Laberg, J.S., Long, D., Mienert, J., Trincardi, F., Urgeles, R., Vorren, T.O., Wilson, C., 2004. Triggering mechanisms of slope instability processes and sediment failures on continental margins: a geotechnical approach. Mar. Geol. 213, 291–321.
Sun, Q.L., Wu, S.G., Cartwright, J., Dong, D.D., 2012. Shallow gas and focused fluid flow systems in the Pearl River Mouth Basin, northern South China Sea. Mar. Geol. 315-318, 1–14.
Sun, Q.L., Alves, T., Xie, X.N., He, J.X., Li, W., Ni, X.L., 2017. Free gas accumulations in basal shear zones of mass-transport deposits (Pearl River Mouth Basin, South China Sea): an important geohazard on continental slope basins. Mar. Pet. Geol. 81, 17–32.
Symons, W.O., Sumner, E.J., Tailing, P.J., Cartigny, M.J.S., Clare, M.A., 2016. Large-scale sediment waves and scours on the modern seafloor and their implications for the prevalence of supercritical flows. Mar. Geol. 371, 130–148.
Talling, P.J., Allin, J., Armitage, D.A., Arnott, R.W.C., Cartigny, M.J.B., Clare, M.A., Felletti, F., Covault, J.A., Girardclos, S., Hansen, E., Hill, P.R., Hiscott, R.N., Hogg, A.J., Clarke, J.H., Jobe, Z.R., Malgesini, G., Mozzato, A., Naruse, H., Parkinson, S., Peel, F.J., Piper, D.J.W., Pope, E., Postma, G., Rowley, P., Sguazzini, A., Stevenson, C.J., Sumner, E.J., Sylvester, Z., Watts, C., Xu, J., 2015. Key future directions for research on turbidity currents and their deposits. J. Sediment. Res. 85, 153–169.
Taylor, B., Hayes, D.E., 1980. The tectonic evolution of the South China Basin. In: Hayes, D.E. (Ed.), The Tectonic and Geologic Evolution of Southeast Asian Seas and Islands, Am. Geophys. Union Monogr. vol. 23. pp. 89–104.
Urlaub, M., Geersen, J., Krastel, S., Schwenk, T., 2018. Diatom ooze: crucial for the generation of submarine mega-slides? Geology 46, 331–334.
Wynn, R.B., Stow, D.A.V., 2002. Classification and characterisation of deep-water sediment waves. Mar. Geol. 192, 7–22.
Wynn, R.B., Weaver, P.P.E., Ercilla, G., Stow, D.A.V., Masson, D.G., 2000. Sedimentary processes in the Selvage sediment-wave field, NE Atlantic: new insights into the formation of sediment waves by turbidity currents. Sedimentology 47, 1181–1197.
Xie, X.N., Müller, R.D., Li, S., Gong, Z.S., Steinberger, B., 2006. Origin of anomalous subsidence along the Northern South China Sea margin and its relationship to dynamic topography. Mar. Pet. Geol. 23, 745–765.
Yang, Q.X., Tian, J.W., Zhao, W., 2010. Observation of Luzon Strait transport in summer 2007. Deep-Sea Res. I Oceanogr. Res. Pap. 57, 670–676.
Zhao, Z.X., Klemas, V., Zheng, Q.N., Yan, X.H., 2004. Remote sensing evidence for baroclinic tide origin of internal solitary waves in the northeastern South China Sea. Geophys. Res. Lett. 31.
Zhao, Y.L., Liu, Z.F., Zhang, Y.W., Li, J.R., Wang, M., Wang, W.G., Xu, J.P., 2015. In situ observation of contour currents in the northern South China Sea: applications for deepwater sediment transport. Earth Planet. Sci. Lett. 430, 477–485.
Zhu, W.L., Huang, B.J., Mi, L.J., Wilkins, R.W.T., Fu, N., Xiao, X.M., 2009. Geochemistry, origin, and deep-water exploration potential of natural gases in the Pearl River Mouth and Qiongdongnan basins, South China Sea. AAPG Bull. 93, 741–761.
Zhu, M.Z., Graham, S., Pang, X., McHargue, T., 2010. Characteristics of migrating submarine canyons from the middle Miocene to present: Implications for paleoceanographic circulation, northern South China Sea. Mar. Pet. Geol. 27, 307–319.